NANO LETTERS

2005
Vol. 5, No. 6
1087−1091

Integration of Scanning Probes and Ion Beams

A. Persaud,* S. J. Park, J. A. Liddle, and T. Schenkel

E. O. Lawrence Berkeley National Laboratory, Berkeley, California 94720

J. Bokor

E. O. Lawrence Berkeley National Laboratory, Berkeley, California 94720 and Department of Electrical Engineering and Computer Science, University of California, Berkeley, California 94720

I. W. Rangelow

Institute of Microstructure Technologies and Analytics, University of Kassel, Germany

Received March 31, 2005; Revised Manuscript Received April 28, 2005

ABSTRACT

We report the integration of a scanning force microscope with ion beams. The scanning probe images surface structures non-invasively and aligns the ion beam to regions of interest. The ion beam is transported through a hole in the scanning probe tip. Piezoresistive force sensors allow placement of micromachined cantilevers close to the ion beam lens. Scanning probe imaging and alignment is demonstrated in a vacuum chamber coupled to the ion beam line. Dot arrays are formed by ion implantation in resist layers on silicon samples with dot diameters limited by the hole size in the probe tips of a few hundred nm.

Beyond imaging, scanning probes (SP) have been integrated with many surface modification functionalities, such as patterning by anodic oxidation,[1] etching of surfaces through transport of excited particles from a plasma source,[2] and deposition of metal lines through nanostencils.[3,4] Focused ion beams (FIB) of mostly Ga ions are routinely available for patterning of materials at a length scale down to about 10 nm. However, a crucial problem in FIB based ion implantation and pattering results from the need to align the ion beam precisely with an electron beam to avoid ions reaching the sample during alignment imaging.[5,6] In addition, most FIB systems can deliver only a single ion species before timely ion source changes. The integration of a scanning probe with an ion beam allows high resolution, nondestructive imaging of the target, and enables alignment of an ion beam to device features with a few nanometer accuracy. In our setup[7,8] the desired ion beam spot size is achieved with a collimating hole in the cantilever as a final beam limiting aperture. This enables us also to align the implantation or patterning spot with the scanned region by placing the tip at a precise location. Holes in tips with diameters as small as 5 nm have been formed by FIB drilling of a few hundred nm wide holes, followed by hole closing via local thin film deposition.[9] Ion beam transport has been characterized for 30 nm diameter holes in nickel foils.[10]

* Corresponding author. E-mail: apersaud@lbl.gov.

10.1021/nl0506103 CCC: $30.25
Published on Web 05/14/2005

The integration of ion beams with scanning probes is similar to the use of a "dynamic nanostencil" for aligned deposition of sub-100 nm wide metal lines.[3,4] Furthermore, Rangelow et al.[2] have used low energy particles transported through a nanonozzle to locally etch or deposit material. The nanonozzle also functioned simultaneously as an scanning probe tip. Our experiment combines the ability to implant ions with non-invasive scanning probe imaging and alignment.

Figure 1 shows a schematic of our setup. The scanning probe is installed in a vacuum chamber (base pressure 10^{-8} Torr), coupled to an ion beam line. Ion beams can be delivered from two ion sources, a medium current source (few μA) for low energy (1 to 10 keV), low charge state ions (1 to 3+), and a low current source for high charge state ions. The latter is an electron beam ion trap (EBIT), which produces particle pA low emittance (1 mm mrad) beams of any neon-like ion across the periodic table, and bare ions up to Kr^{36+}. We use it here for production of Bi^{45+} beams with a kinetic energy of 180 keV.[11] Bi is a donor in silicon, and a candidate for implementation of electron spin-based quantum computation.[12]

A bending magnet in the beam line is used to select a certain charge state of the used ion species. The beam is focused by several Einzel lenses into an 8 in. cube where a

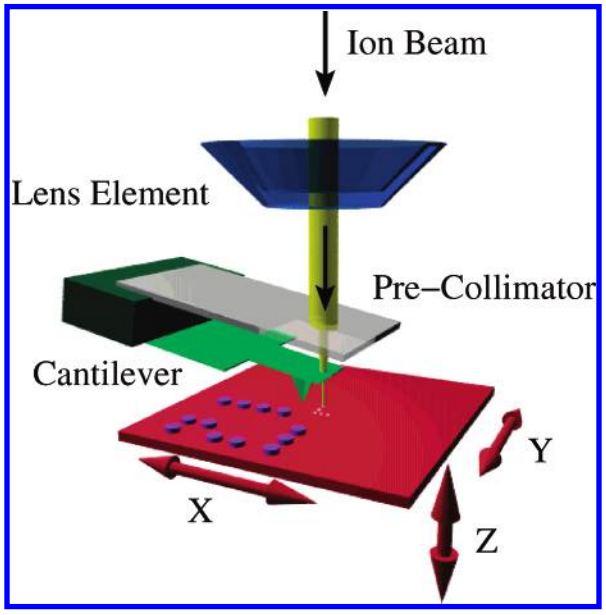

Figure 1. Schematic of the setup. A piezoresistive cantilever with a small hole and an imaging tip is mounted on a pre-collimating aperture in front of an ion beam lens element. The tip can be positioned relative to alignment markers on the sample for ion implantation.

lens element that acts as a beam limiting aperture of 1 mm diameter separates the target area and the scanning probe from the rest of the beam line. The scanning probe tip is mounted behind this aperture on a flexure stage for coarse approach of the tip to the surface and is kept fixed in position during scans and implantation. The target is mounted on a stage with a 100 μm $\times$ 100 μm $\times$ 10 μm range and nanometer precision. Stage motion is used to acquire scan images from the SP or position the sample at specific locations.

Because of space restrictions, the integration of a laser for standard optical detection of the cantilever deflection signal is impractical here. Instead, we use a piezoresistive readout scheme. The silicon cantilevers have a piezoresistive Wheatstone bridge built into the cantilever beam.[13] This and a vacuum preamp stage ($\times$10) result in relatively high signal-to-noise ratios for imaging. The deflection signal is further amplified in a second amplifier stage outside the vacuum chamber, and a low pass filter is applied before the signal is fed into the SP control hardware. Typical signal strengths are a few μV per nm deflection. The cantilevers have a typical spring constant of several *N*/*m*. The dimensions of the beam are about 150 μm $\times$ 600 μm.[14] The cantilever is mounted on a ceramic chip, which can also hold a pre-collimating foil mounted 300−700 μm behind the cantilever to shield the rest of the sample from ion implantation.[8]

The final beam limiting aperture is drilled into the cantilever using a FIB with 30 keV Ga^+ ions. Figure 2 shows scanning electron microscope (SEM) images of the imaging tip and collimating aperture formed on a cantilever. In case of a pre-collimator, holes in the cantilever and the pre-collimator are formed in one drilling step and are therefore self-aligned. Aspect ratio limitations preclude direct drilling of small holes in thick samples. We find that aspect ratios

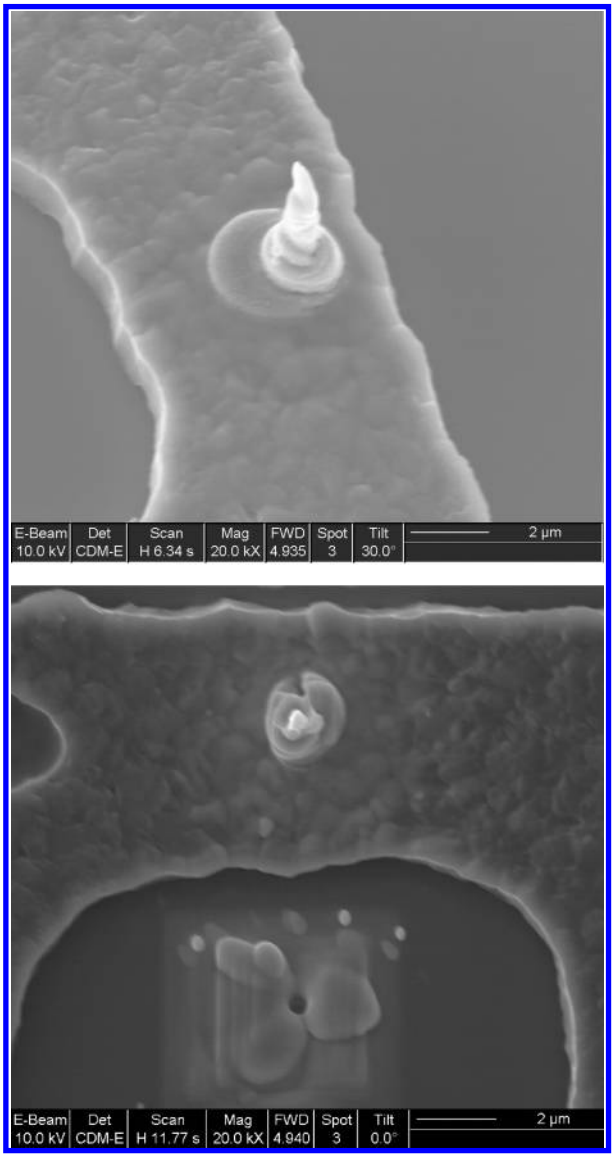

Figure 2. SEM images of the AFM tip (top) and the collimating aperture (below), both formed by ion beam assisted Pt deposition in a FIB on a piezoresistive scanning probe sensor. The aperture diameter is 300 nm, and the radius of curvature is estimated to be $<$ 100 nm.

are limited to about 5:1 in FIB drilling of micrometer thick cantilevers. Smaller hole diameters are achieved by closing micron size holes via ion (or electron) beam assisted platinum deposition.[9] A thin metal film first closes the micron-sized hole, and a second hole is then drilled into the Pt film. This process of hole closing and re-drilling can be repeated until the desired hole size is reached. It is important here that the Pt film is thick enough to stop ions, and a few hundred nanometer film thickness suffices to stop the ions used in this study. Required stopping ranges can be estimated by SRIM.[15] A Pt film with a thickness of only 100 nm will efficiently stop 50 keV Ar and 200 keV Bi ions.

Ion beam assisted Pt deposition was also used to build SP tips onto the cantilever in a defined distance to the drilled hole.[8] Details of the SP setup with FIB processed cantilevers have been reported elsewhere.[8] From the SEM images, the radius of curvature for the tips can be estimated to a size

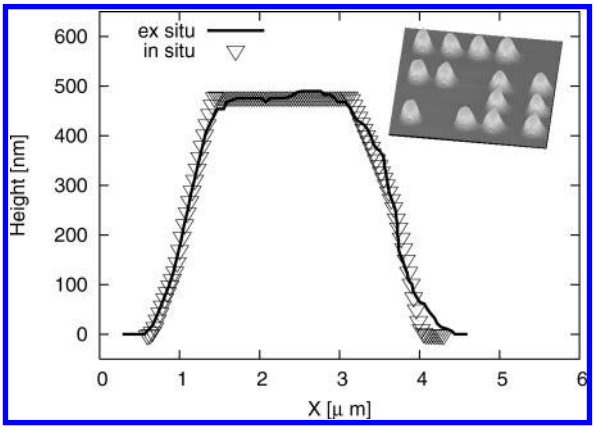

Figure 3. Line scan of a 2 μm wide alignment markers on a silicon sample is taken in situ (10^{-7} Torr) with the tip shown in Figure 2. The inset shows a 24 × 24 μm^2 scan of a marker sample, acquired under the same conditions. Also shown is an ex situ line scan of the same dot acquired with a commercial AFM.

smaller than 100 nm. From a comparison of line scans across identical features on a calibrated sample with a commercial tip and AFM, we believe that the actual tip radius is much smaller, comparable with commercial tips.

Evidently, sputtering will alter and eventually destroy thin collimators, and FIB-formed Pt tips were found to blunt after several hours of imaging in vacuum. Cantilevers can be refurbished reliably, and tips and holes have been regrown several times on the cantilever shown here. Inspection with SEM found holes to be stable after extended beam exposures (>10 *h* with ≈ 1 nA/mm^2 Ar^{2+} intensities).[8]

The effective resolution in local ion implantation and doping or pattering with ion beams is limited by the collimator diameter, possible beam broadening in the interaction of ions with the small hole (slit scattering), and also by range straggling of implanted ions.[10] An SP imaging resolution of a few nm is therefore sufficient in this instrument, and this also relaxes the requirements for the sharpness of FIB formed tips.

The results reported in this letter were produced using silicon cantilevers with a series of four holes: two 4 μm sized holes, one hole with a 1 μm diameter, and one hole with a diameter of 300 nm achieved by closing down a bigger hole with platinum deposition and then re-drilling the hole in the platinum. The holes were places approximately 50 μm apart.

The image in Figure 3 shows a line scan across a 2 μm wide alignment dot formed by standard microfabrication techniques on a silicon surface using the tip shown in Figure 2. The surface roughness determined with this tip is about 1 nm over a (15 μm)^2 area, and comparison of a line scan of one these markers with imaging results, using a commercial AFM at air, lets us estimate an imaging resolution of better than 10 nm. For the ion implantation and pattering experiments, the tip was positioned 10 μm above the target surface. Implantation in contact mode is also possible. We did not observe effects on image quality when the ion beam was on during imaging. The sample stage was programmed to move to a specific position and stay there for a fixed dwell time

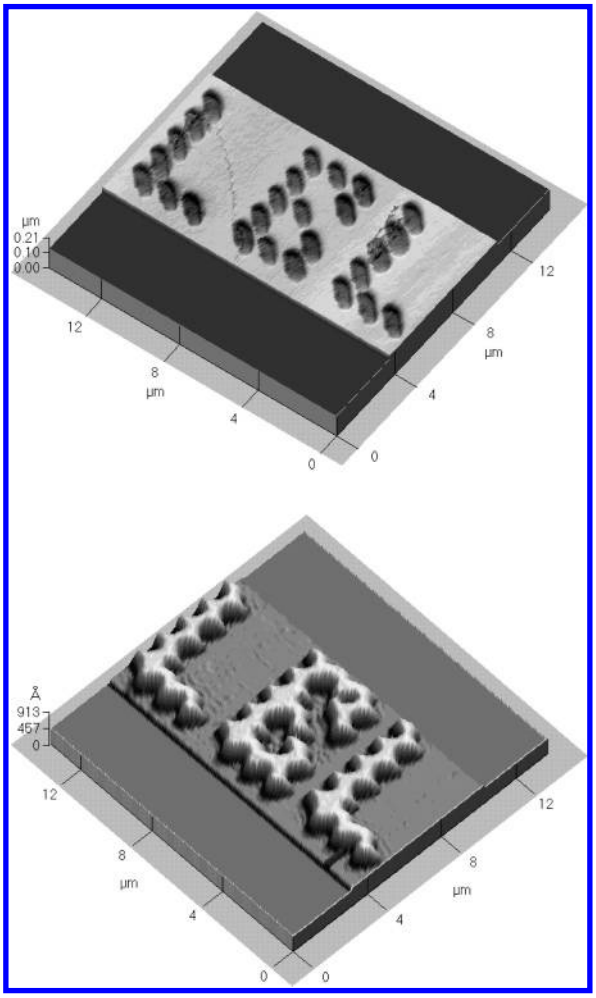

Figure 4. Ex situ AFM image of a pattern formed in resist by ion implantation with scanning probe alignment. Ions used here were 7 keV Ar^{2+}. Top: PMMA (using the cantilever shown in Figure 2). Bottom: HSQ.

before moving to the next defined point. The dwell time was set to 10 s per spot for exposures with a 2 nA/mm^2Ar^{2+} beam (6 keV), and the translation speed between points was set to 100 μm/s.

We used poly(methyl methacrylate) (PMMA, positive tone) and hydrogen silsesquioxane (HSQ, negative tone) as resists on silicon wafers for demonstration of pattern formation. The PMMA (molecular weight 495 k) was spun onto a silicon wafer resulting in a 50 nm high film (prebaked at 60 °C for one minute). The thickness of the HSQ film was also about 50 nm. Markers were imaged and an off marker area was selected with the SP. The equivalent argon ion dose per dot was approximately 10^{13} cm^{-2} (or several μC[16]).

An image of the dot pattern formed by aligned implantation through the 300 nm hole (Figure 2) is shown in Figure 4 after resist development. The slightly oval dot shape is due to the low beam quality of the Ar-beam and was also visible for larger hole sizes, but is not visible when using the low emittance beam from the EBIT source (see Figure 5).

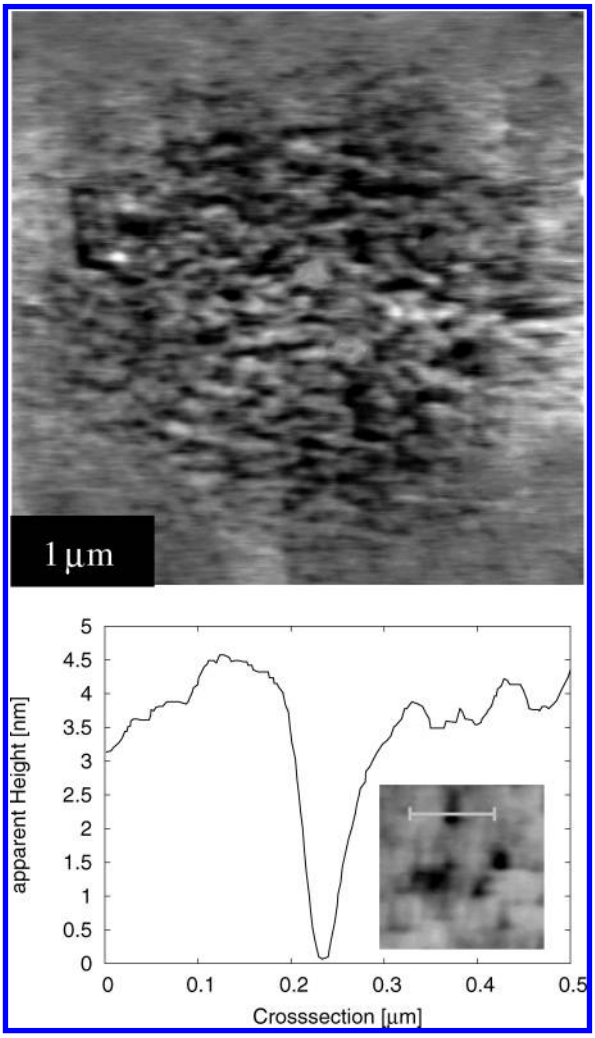

Figure 5. Ex situ scanning probe image of a 4 μm wide spot were PMMA was exposed with Bi^{45+} ions (180 keV) (top). Below: Ex situ scanning probe image and line out of a single ion impact site (after resist development).

A pattern formed in HSQ is shown in Figure 4. As with the PMMA sample, each spot was exposed several times. The results with a few hundred nm wide holes are similar for PMMA (positive tone) and HSQ (negative tone), but HSQ is expected to yield higher resolution for smaller feature sizes.[17]

In Figure 5, we show an ex situ AFM image of a 4 μm wide dot exposed to highly charged Bi ions (Bi^{45+}, 180 keV) on a PMMA sample. The high charge state significantly enhances the resist developing power of single ions,[18,19] and impact sites where the resist was exposed by single ions can be resolved. Figure 5 also shows a single ion hit site with a diameter of about 50 nm. Here, the hole in the resist on silicon is now aligned to the position of a single donor atom that is implanted at a depth of about 40 nm in the silicon. The placement uncertainty from straggling is about 11 nm, the same as for 15 keV P ions.[15,21] The asymmetric scattering kinematics of the Bi−Si system leads to significantly reduced straggling, compared to the symmetrical scattering of P on Si. The single ion induced defect sites are self-aligned with the implanted ion and allow the aligned formation of device structures.

Ion beam transport through 300 nm wide holes in cantilevers formed reproducible, aligned dots. The integration of a scanning probe with ion beams enables the doping of selected device areas. Throughput could be increased with multiple cantilevers. When integrated with a single ion detection scheme, this technique enables formation of devices that are doped with defined numbers of atoms. Single ion detection can be achieved by detection of secondary electrons from single ion impacts,[10,20,6] or through collection of electron−hole pairs formed by implanted ions inside the solid.[21] Single ion signals in both secondary electron emission and excitation in the solid are very strongly enhanced for highly charged dopant ions.[10,20,22]

Examples of proposed single atom devices are quantum computers based on coherent manipulation of electron and nuclear spins of donor atoms,[12,23] or excited states of single atoms.[24−26] Ion placement resolution requirements in quantum computer schemes depend on specific architectures and range from approximately 10 nm for electron spin proposals,[12,27] to several hundred nm for defect centers in diamond with optical control. Atomic[28] or even one nm scale placement resolution would require use of very low energy ions and nanotube like collimators.

In conclusion, we report first results from the integration of a scanning probe with an ion beam. Aligned ion implantation is demonstrated by the formation of dot patterns in resist on silicon. An imaging resolution and alignment accuracy of $\leq$10 nm was achieved with FIB processed tips. Dot sizes are limited by the hole diameters of 300 nm. This technique enables local doping of materials and devices and can be combined with single ion detection for aligned single ion implantation. Tests of placement resolution limits with sub-100 nm diameter holes are in progress.

Acknowledgment. We thank the staffs of the UC Berkeley Microlab and the National Center for Electron Microscopy at LBNL for their support. This work was supported by NSA and ARDA under ARO contract number MOD707501, and by the U.S. DOE under contract number DE-AC03-76SF00098.

References

(1) Snow, E. S.; Campbell, P. M. *Science* **1995**, *270*, 1639.
(2) Rangelow, I. W.; Voigt, J.; Edinger, K. *J. Vac. Sci. Technol. B* **2001**, *19*(6), 2723.
(3) Lüthi, R.; Schlittler, R. R.; Brugger, J.; Vettiger, P.; Welland, M. E.; Gimzewski, J. K. *Appl. Phys. Lett.* **1999**, *75*, 1314.
(4) Egger, S.; Ilie, A.; Fu, Y.; Chongsathien, J.; Kang, D. J.; Welland, M. E. *Nano Lett.* **2005**, *5*(1), 15.
(5) Shen, T. C.; Kline, J. S.; Schenkel, T.; Robinson, S. J.; Ji, J. Y.; Yang, C.; Du, R. R.; Tucker, J. R. *J. Vac. Sci. Technol. B* **2004**, *22*(6), 3182.
(6) Shinada, T.; Koyama, H.; Hinoshita, C.; Imamura, K.; Ohdomari, I. *Jpn. J. Appl. Phys.* **2002**, *41*, L287.
(7) Persaud, A.; Park, S. J.; Liddle, J. A.; Rangelow, I. W.; Bokor, J.; Keller, R.; Allen, F. I.; Schneider, D. H.; Schenkel, T. *Quantum Info. Process.* **2004**, *3*, 233.
(8) Persaud, A.; Allen, F. I.; Gicquel, F.; Park, S. J.; Liddle, J. A.; Schenkel, T.; Ivanov, Tzv.; Ivanova, K.; Rangelow, I. W.; Bokor, J. *J. Vac. Sci. Technol. B* **2004**, *22*(6), 2992.
(9) Schenkel, T.; Radmilovic, V.; Stach, E. A.; Park, S. J.; Persaud, A. *J. Vac. Sci. Technol. B* **2003**, *21*(6), 2720.
(10) Schenkel, T.; Persaud, A.; Park, S. J.; Nilsson, J.; Bokor, J.; Liddle, J. A.; Keller, R.; Schneider, D. H.; Cheng, D. W.; Humphries, D. E. *J. Appl. Phys.* **2003**, *94* (11), 7017.

(11) Schenkel, T.; Hamza, A. V.; Holder, J. P.; Krämer, K.; McDonald, J. W.; Persaud, A.; Schneider, D. H. *Rev. Sci. Instrum.* **2002**, *73*(2), 663.
(12) De Sousa, R.; Delgado, J. D.; das Sarma, S. *Phys. Rev. A* **2004**, *70*(5), 052304.
(13) Gotszalk, T.; Grabiec, P.; Rangelow, I. W. *Ultramicroscopy* **2003**, *97*(1−4), 385.
(14) Pedrak, R.; Ivanov, Tzv.; Ivanonva, K.; Gotszalk, T.; Abedinov, N.; Rangelow, I. W.; Edinger, K.; Tomerov, E.; Schenkel, T.; Hudek, P. *J. Vac. Sci. Technol. B* **2003**, *21*(6), 3102.
(15) SRIM: Stopping and range of ions in matter, http://www.srim.org/.
(16) Karapiperis, L.; Dubreuil, D.; David, Ph.; Dieumegard, D. *J. Vac. Sci. Technol. B* **1985**, *3*, 353.
(17) Namatsu, H.; Takahashi, Y.; Yamazaki, K.; Yamaguchi, T.; Nagase, M.; Kurihara, K. *J. Vac. Sci. Technol. B* **1998**, *16*(1), 69.
(18) Gillaspy, J. D.; Parks, D. C.; Ratliff, L. P. *J. Vac. Sci. Technol. B* **1998**, *16*(6), 3294.
(19) Schenkel, T.; Schneider, M.; Hattass, M.; Newman, M. W.; Barnes, A. V.; Hamza, A. V.; Schneider, D. H.; Cicero, R. L.; Chidsey, C. E. D. *J. Vac. Sci. Technol. B* **1998**, *16*(6), 3298.
(20) Park, S. J.; Persaud, A.; Liddle, J. A.; Nilsson. J.; Bokor. J.; Schneider, D. H.; Rangelow, I. W.; Schenkel, T. *Microelectr. Eng.* **2004**, *73*−*74*, 695.
(21) Jamieson, D. N.; Yang, C.; Pakes, C. I.; Hearne, S. M.; Prawer, S.; Stanley, F. E.; Dzurak, A. S.; Clark, R. G. *AIP* **2003**, *CP680*, 561. Yang, C. Y.; Jamieson, D. N.; Pakes, C.; Prawer, S.; Dzurak, A.; Stanley, F.; Spizziri, P.; Macks, L.; Gauja, E.; Clark, R. G. *Jpn. J. App. Phys.* **2003**, *42* (6B), 4124.
(22) Schenkel, T.; Barnes, A. V.; Niedermayr, T. R.; Hattass, M.; Newman, M. W.; Machicoane, G. A.; McDonald, J. W.; Hamza, A. V.; Schneider, D. H. *Phys. Rev. Lett.* **1999**, *83*(21), 4273.
(23) Kane, B. E. *Nature* **1998**, *393*, 133.
(24) Jelezko, F.; Gäbel, T.; Popa, I.; Domhan, M.; Gruber, A.; Wrachtrup, J. *Phys. Rev. Lett.* **2004**, *93*(13), 130501.
(25) Golding, B.; Dykman, M. I. *arXiv: cond-mat/0309147* **2003**. Smelyanskiy, V. N.; Petukhov, A. G.; Osipov, V. V.; *arXiv: quant-ph/0407220* **2004**.
(26) Stoneham, A. M.; Fisher, A. J.; Greenland, P. T. *J. Phys.: Condens. Matter* **2003**, *15*(27), L447.
(27) Skinner, A. J.; Davenport, M. E.; Kane, B. E. *Phys. Rev. Lett.* **2003**, *90*(8), 087901.
(28) O'Brien, J. L.; Schofield, S. R.; Simmons, M. Y.; Clark, R. G.; Dzurak, A. S.; Curson, N. J.; Kane, B. E.; McAlpine, N. S.; Hawley, M. E.; Brown, G. W. *Phys. Rev. B* **2001**, *64*(16), 161401.

NL0506103